Applied Surface Science 582 (2022) 152480

Contents lists available at ScienceDirect

Applied Surface Science

journal homepage: www.elsevier.com/locate/apsusc

Full Length Article

Conducting interfaces between $LaAlO_3$ and thick homoepitaxial $SrTiO_3$ films for transferable templates

Jung-Woo Lee [a,b,1], Jongmin Lee [c,1,2], Jamin Ahn [c], Hongji Yoon [c], Hyunji An [c], Sang-Il Park [d], Hong-Seok Kim [d], Sehun Seo [c], Yong-Joo Doh [d], Wooyoung Lee [a,b], Sangwoo Ryu [e,*], Sanghan Lee [c,*]

[a] Department of Materials Science and Engineering, Yonsei University, Seoul 03722, Republic of Korea
[b] KIURI Institute, Yonsei University, Seoul 03722, Republic of Korea
[c] School of Materials Science and Engineering, Gwangju Institute of Science and Technology, Gwangju 61005, Republic of Korea
[d] Department of Physics and Photon Science, Gwangju Institute of Science and Technology, Gwangju 61005, Republic of Korea
[e] Department of Advanced Materials Engineering, Kyonggi University, Suwon 16227, Republic of Korea

ARTICLE INFO

Keywords:
Complex oxide membranes
$SrTiO_3$
Two-dimensional electron gas
Pulsed laser deposition

ABSTRACT

For the mechanical stability of heterostructure membranes such as $LaAlO_3$ (LAO)/$SrTiO_3$ (STO), which is well-known for two-dimensional electron transport at the interface, a thick template substrate layer is required. However, thick STO films typically suffer from the formation of undesired point defects, mainly due to its cation off-stoichiometry, which results in the insulating interface with LAO. Herein, we report the successful fabrication of a conducting interface between LAO and thick homoepitaxial STO films by pulsed laser deposition. The careful optimization of laser ablation parameters including laser energy density and laser spot size led to stoichiometric 500 nm–thick STO films that have a lattice structure identical to that of bulk single crystals of STO, as confirmed by X-ray diffraction and temperature-dependent Raman spectroscopy. The interface between 4 nm–thick LAO and 500 nm–thick stoichiometric STO films exhibited a metallic behavior at low temperature down to 4 K, implying a low concentration of point defects in the homoepitaxial STO film. Ultimately, a crack-free, millimeter-sized 500 nm–thick STO membrane was successfully fabricated. These results are expected to facilitate the integration of high-quality complex oxide heterostructure membranes with various substrates including silicon, enabling their practical applications.

1. Introduction

Complex oxide heterostructures have attracted significant attention owing to their novel emergent phenomena such as gate-tunable superconductivity, magnetic skyrmions, and fractional quantum Hall effect [1–3]. One of the representative examples is the formation of a two-dimensional electron gas (2DEG) at the interface between two band insulators such as $LaAlO_3$ (LAO) and $SrTiO_3$ (STO) [4]. This novel interface has intrigued researchers because it not only shows emergent phenomena [1,4–6] but also has potential for applications in electronic devices [7,8]. One of the issues in this interface is to incorporate this material platform into existing silicon technologies to realize a wider range of applications [9,10]. There are some reports on the epitaxial growth of STO on a Si substrate [10–15]. However, because the formation of oxides at a Si surface prevents the growth of single-crystalline STO films, limited methods such as molecular beam epitaxy (MBE) [10–15], even with particular pre-treatments [13], are necessary to obtain high-quality STO films. Furthermore, the large lattice mismatch of ~1.7% between Si and STO results in the formation of dislocations, which can deteriorate the intrinsic transport properties of STO-based

* Corresponding authors at: School of Materials Science and Engineering (SMSE) / Gwangju Institute of Science and Technology (GIST), 123 Cheomdangwagi-ro, Buk-gu, Gwangju 61005, Republic of Korea. Department of Advanced Materials Engineering, Kyonggi University, 154-42, Gwanggyosan-ro, Yeongtong-gu, Suwon-si, Gyeonggi-do 16227, Republic of Korea.
E-mail addresses: sryu@kyonggi.ac.kr (S. Ryu), sanghan@gist.ac.kr (S. Lee).
[1] These authors contributed equally to this work.
[2] Present address: Department of Materials Science & Engineering and Materials Research Laboratory, University of Illinois at Urbana-Champaign, Urbana, Illinois 61801, United States

https://doi.org/10.1016/j.apsusc.2022.152480
Received 1 November 2021; Received in revised form 28 December 2021; Accepted 8 January 2022
Available online 11 January 2022

heterostructures [10].

Recently, a new approach using freestanding membranes was proposed [16]. The layer transfer method has been typically used for two-dimensional materials such as graphene [17,18] and MoS_2 [19,20]. Although the transfer of oxide thin films is challenging owing to their weak mechanical properties, the transfer of various types of complex oxide membranes including STO [16], $La_{0.7}Sr_{0.3}MnO_3$ [16], $SrRuO_3$ [21], and $YBa_2Cu_3O_{7-\delta}$ [22] has been demonstrated while preserving their intrinsic properties.

The next step should be the transfer of multi-layer thin films, *i.e.*, heterostructures. However, this process is more challenging because heterostructure membranes tend to bend because of their internal strain, which originates from the lattice mismatch between two different layers [23]. To obtain flat heterostructure membranes, thick template layers are necessary. For example, based on the lattice mismatch between LAO (a_{pc} = 3.787 Å, where pc stands for pseudo-cubic) and STO (a = 3.905 Å), it has been reported that an STO layer approximately 200 nm in thickness is necessary for holding a 10 unit cell (u.c.) LAO layer on top without bending [23]. One problem with thick STO films is that they typically possess undesired point defects, which deteriorate the electron mobility at LAO/STO heterointerfaces [24,25]. There are few reports on conducting interfaces between LAO and a homoepitaxial STO film fabricated by pulsed laser deposition (PLD); in these reports, the STO layer thickness is limited to less than ~16 nm, or a high growth temperature of 1100 °C is used for thicker STO films [24]. This is a drawback for practical device applications.

Herein, we demonstrate the successful fabrication of a conducting interface between LAO and thick homoepitaxial STO films through careful optimization of the PLD process. As key factors to obtain a conducting interface, we identified not only well-known thermodynamic parameters such as growth temperature and oxygen pressure during the film growth, but also parameters related to the laser ablation including the laser energy density and laser spot size on the STO target surface. The fully optimized stoichiometric 500 nm–thick STO film has the same lattice structure as a bulk single crystal of STO, as confirmed by X-ray diffraction (XRD) and temperature-dependent Raman spectroscopy. The metallic interface is maintained at low temperature down to 4 K, indicating a low concentration of defects in the optimized STO film. Furthermore, using $SrRuO_3$ (SRO) as a sacrificial layer, high-quality 500 nm–thick STO membranes having dimensions of the order of millimeters were successfully fabricated without cracking issues.

2. Experimental

2.1. Preparation of heterostructures

STO and LAO films were grown by PLD using a KrF excimer laser (Coherent Inc. COMPexPro 205F, pulse duration = 20 ns) on (001)-oriented STO single-crystal substrates (Shinkosha, CrysTec GmbH). STO (001) substrates were etched in a buffered HF (BHF) solution for 60 s and subsequently annealed at 1000 °C for 40 min in an oxygen atmosphere to obtain an atomically smooth, TiO_2-terminated surface. Homoepitaxial STO films with a thickness ranging from 20 nm to 500 nm were grown on either untreated or BHF-treated (001) STO substrates using a single-crystal STO target. A growth temperature of 750 °C, an oxygen pressure of 13.3 Pa, a laser pulse repetition rate of 5 Hz, and a target-to-substrate distance of 55 mm were employed. To optimize the laser ablation conditions, the laser spot size on the target surface was carefully measured and tuned by changing the position of the focus lens and the mask size. The details are presented in Fig. S1 and Table S1. The laser energy density was also varied in the range of 1.0–3.0 J/cm^2. Thus, 4 nm–thick LAO films were deposited on the homoepitaxial STO films without breaking vacuum, and LAO films with the same thickness were grown on STO (001) single-crystal substrates for comparison. A growth temperature of 550 °C and an oxygen pressure of 0.133 Pa were used for the LAO growth. A single-crystalline LAO target was ablated with a laser energy density of ~1.0 J/cm^2 at a repetition rate of 3 Hz. After LAO deposition, LAO/homoepitaxial STO/STO heterostructures were cool down to room temperature, keeping the oxygen pressure at 0.133 Pa.

2.2. Preparation of STO membranes

$SrRuO_3$ (SRO) was used as a sacrificial layer for preparing STO membranes. 30 nm–thick SRO layers were deposited on STO (001) substrates, and 500 nm–thick STO films were grown on top of the SRO. A growth temperature of 550 °C, an oxygen pressure of 13.3 Pa, a laser energy density of ~2.0 J/cm^2, and a repetition rate of 3 Hz were used for SRO growth. Supporting layers such as polymethyl methacrylate (PMMA), polydimethylsiloxane (PDMS), or polyimide (Kapton tape) were attached to the surface of STO/SRO/STO substrate heterostructures, following which the samples were immersed in a 0.4 M $NaIO_4$ solution to remove the SRO layer at an etching rate of ~2 nm/s. After the removal of the SRO layer, STO membranes attached to the supporting layer were obtained.

2.3. Characterization

The crystal structures of films and heterostructures were analyzed by X-ray diffraction (XRD) using a PANalytical X'Pert Pro diffractometer with Cu Kα radiation (λ = 1.5406 Å). Temperature-dependent Raman spectroscopy was performed using a LabRam HR800 UV Raman microscope (Horiba Jobin-Yvon, France) with a 325 nm He-Cd laser at KBSI, Gwangju-center. The spectra were taken in the temperature range of 77–300 K with a LinKam sample stage. Hall measurement was performed for characterizing transport properties such as the sheet resistance, carrier density, and electron mobility of 2DEG at the interface between LAO and STO by using the van der Pauw geometry. To observe the surface of the STO membrane, field-emission scanning electron microscopy (FE-SEM, Hitachi S-4700) was performed at Korea Photonics Technology Institute.

3. Results and discussion

Fig. 1a schematically shows the strategy for obtaining stoichiometric STO films and conducting interfaces with LAO on top by controlling the critical laser parameters of the PLD process. We chose an STO (001) single crystal as a substrate to rule out any strain effect on stoichiometric STO films [26]. Because the transport channel exists on the STO side (~10 nm) of the interface [6], the control of point defects that can act as scattering centers [27–29] in STO films is directly related to the electrical properties of LAO/STO heterointerfaces. In the case of STO, cation off-stoichiometry is one of the major sources of extra point defects in the films, such as V_{Sr}, Ti_{Sr}, Sr_{Ti}, and V_O [27,30–33]. Although many research groups have attempted to minimize point defects by controlling cation stoichiometry in the film [27,30,34], the growth window was found to be very narrow [27,35], and consequently, LAO/PLD-grown thick STO heterointerfaces are often insulating [25]. As shown in (Fig. 1b), laser parameters including the laser energy density and laser spot size on the PLD target [36], as well as thermodynamic parameters such as the substrate temperature and oxygen partial pressure during the film growth, are critical to achieve a conducting interface between LAO and homoepitaxial STO. Because this cation off-stoichiometry causes the volume expansion of the STO unit cell [37,38], one can determine whether the STO film is stoichiometric by analyzing the peak position in the XRD patterns. Fig. 1c shows the XRD patterns of LAO (4 nm)/STO (500 nm)/STO (001) substrate. The pattern of LAO (4 nm)/STO (001) substrate is also provided for reference. While there is no difference in the STO peak position when using a laser energy of 1 J/cm^2 and laser spot size of 1.8 mm^2, the STO (002) peak is shifted with respect to the bulk counterpart in off-stoichiometric STO films grown with a higher laser energy of 3 J/cm^2 and the same laser spot size. With a fixed laser

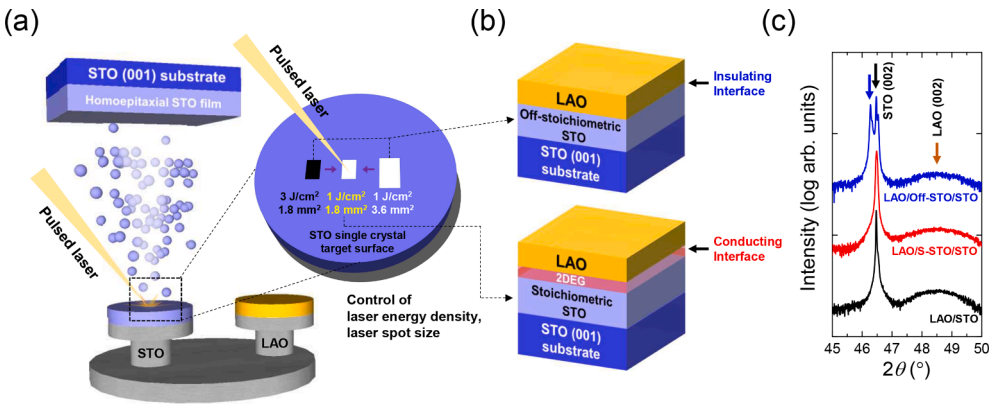

Fig. 1. (a) Schematic of the strategy for obtaining stoichiometric STO films using a PLD system for conducting LAO/STO heterostructures. The laser energy density and laser spot size on the STO target have been optimized for the growth of stoichiometric STO films. The optimization process is detailed in Fig. S1 and Table S1. (b) Schematic of LAO/STO heterostructures with off-stoichiometric and stoichiometric STO films on STO (001) substrates, resulting in an insulating and a conducting interface, respectively. (c) Out-of-plane θ-2θ XRD patterns of samples where 4 nm–thick LAO films were grown on stoichiometric (S-STO) and off-stoichiometric STO films (Off-STO) on STO (001) substrates. Note that laser energies of ~1.0 J/cm^2 and ~3.0 J/cm^2 were used for S-STO and Off-STO, respectively. The XRD pattern of an LAO film directly grown on an STO substrate is also shown for comparison. The black and blue arrows indicate the ideal peak position of STO (002) and the (002) peak position shifted by off-stoichiometry in the STO film, respectively. The LAO (002) peak position is indicated by the brown arrow.

energy of 1 J/cm^2, we carefully tuned the laser spot size on the target surface as shown in Fig. S1a. Detailed information on the lens position and mask size is provided in Table S1. At the same energy density of 1 J/cm^2, a spot size of 1.8 mm^2 was found to be suitable for stoichiometric films. With a larger spot size of 3.6 mm^2, the distinct STO (002) reflection is observed from the film (Fig. S1b), indicating the off-stoichiometry of the STO film. The principle of tuning the stoichiometry in STO by changing the laser energy density and laser spot size is that there is a different spatial distribution of SrO and TiO_x components in STO plasma plume [39]. Thus any change in shape or size of the plume at certain target-to-substrate distance can affect the film stoichiometry.

To further confirm the stoichiometry of the STO films, temperature-dependent Raman spectroscopy was employed. Because the ideal STO has a cubic perovskite structure (space group $Pm\bar{3}m$, No. 221) [40], its twelve optical phonon modes have odd symmetry with respect to the inversion center, rendering the first-order Raman scattering inactive [41]. However, any cation off-stoichiometry, irrespective of whether it is Sr- or Ti-rich, is known to break the inversion symmetry of STO, resulting in first-order peaks in Raman spectra such as LO_3, LO_4, or TO_4 modes [42]. Fig. 2a shows the Raman spectra of an STO substrate, a stoichiometric film, and an off-stoichiometric film measured at 300 K. While there is no difference in spectra between the STO substrate and stoichiometric film, a first order peak is observed in the off-stoichiometric film. This observation is more dramatic at a low temperature of 77 K (Fig. 2b), confirming the defect-induced structural distortion originating from cation off-stoichiometry [42]. The full spectra of each sample in the temperature range of 77–300 K are shown in Fig. S2.

The electrical transport properties of three heterostructures, where LAO was grown on an STO substrate (LAO/STO), a stoichiometric STO film (LAO/S-STO/STO), or an off-stoichiometric STO film (LAO/Off-STO/STO), are compared in Fig. 3. As shown in Fig. 3a, the reference LAO/STO heterostructure exhibits a metallic behavior at temperatures below 10 K, similar to previous reports [4–6]. However, LAO/Off-STO/STO shows an insulating behavior, indicating dominant defect scattering in the STO layer [29]. The LAO/S-STO/STO heterostructure exhibits a metallic behavior down to 4 K, but the sheet resistance value at low temperature (<10 K) is approximately 8 times higher than that of the reference LAO/STO heterostructure. This is attributed to the lower mobility at LAO/S-STO/STO (Fig. 3c), rather than its carrier concentration (Fig. 3b). Notably, the carrier concentration in LAO/S-STO/STO is higher than that in LAO/STO in the temperature range of 4–300 K. This is probably due to oxygen vacancy formation in the STO films during the growth because no post-growth annealing was performed on the STO films. The mobility of LAO/S-STO/STO at low temperature (<10 K) is about one order lower than that of LAO/STO, implying that the defect concentration in the stoichiometric STO film is still higher than that in the bulk single crystal, although they are structurally identical within the resolution of XRD [43] and Raman spectroscopy.

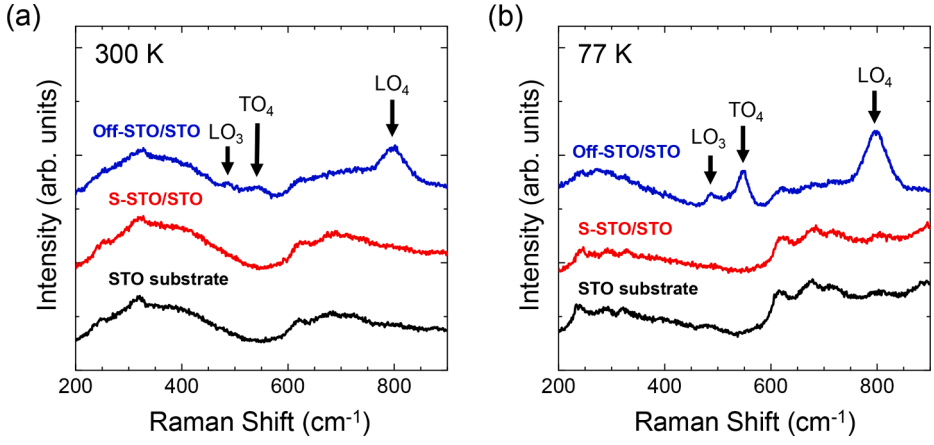

Fig. 2. Raman spectra of a stoichiometric and an off-stoichiometric STO film grown on STO (001) substrates as well as an STO substrate, measured at (a) 300 K and (b) 77 K. The peaks related to the LO_3, TO_4, and LO_4 first-order phonon modes are marked by arrows. A stoichiometric and an off-stoichiometric STO film with 250 nm in thickness were grown using a laser energy density of 1 and 2 J/cm^2, respectively, with a fixed laser spot size of 1.8 mm^2.

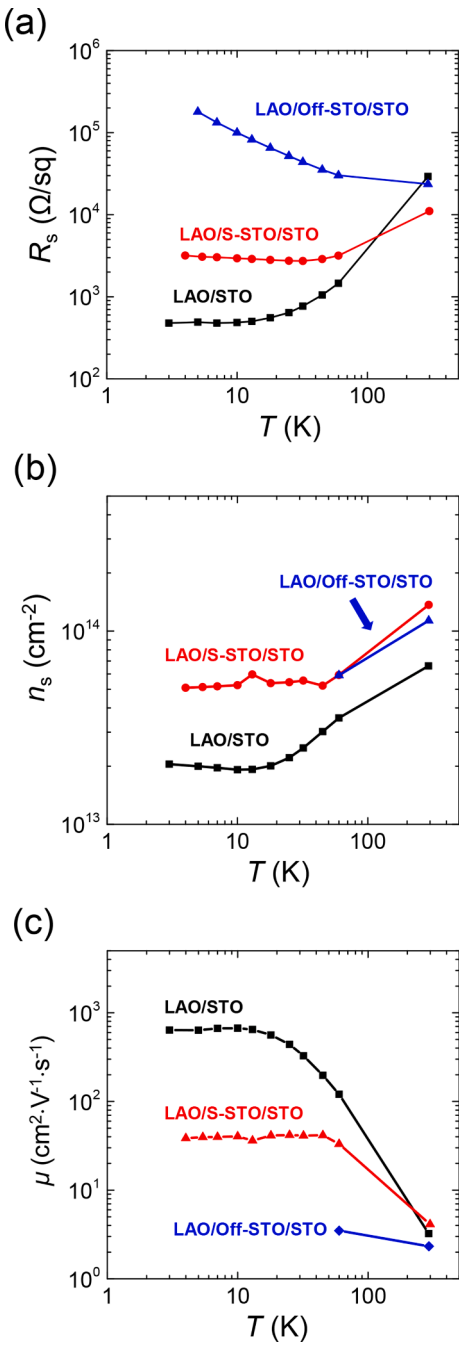

Fig. 3. Transport properties of 2DEG at the interfaces of LAO/STO substrate and LAO/homoepitaxial STO/STO substrate: temperature dependency of (a) sheet resistance (R_s), (b) 2D carrier concentration (n_s), and (c) electron mobility (μ). Note that the carrier concentration and mobility values were not evaluated at temperatures below 60 K in the LAO/Off-STO/STO substrate sample owing to nonlinearity and noise in the Hall signal, which originated from the high sheet resistance in this temperature region.

Nonetheless, it should be noted that the mobility value of 39 $cm^2V^{-1}s^{-1}$ at 4 K in LAO/S-STO/STO is about 5 times higher than that in LAO/MBE-grown STO near 10 K [10]. Below 60 K, we were not able to estimate the carrier concentration and mobility from the Hall data of LAO/Off-STO/STO, because of noisy signals due to high resistance. We also checked the effect of thickness of homoepitaxial STO on the electrical properties in LAO/S-STO/STO, as shown in Fig. S3. The interface in LAO (4 nm)/S-STO (20 nm) shows an even lower sheet resistance in the entire temperature range of 3–300 K (Fig. S3a), mainly due to the high carrier concentration (Fig. S3b) originating from additional oxygen vacancy formation during the growth, as mentioned above. The mobility value at 3 K (477 $cm^2V^{-1}s^{-1}$) is comparable to that of the LAO/STO sample (638 $cm^2V^{-1}s^{-1}$), as shown in Fig. S3c. This indicates that even under the optimal growth condition, the mobility was found to decrease with respect to the thickness of the homoepitaxial STO films, probably due to hidden factors such as changes of the target surface during the growth, which must be investigated in future work.

Finally, the feasibility of thick stoichiometric STO membranes was tested using the heterostructure STO (500 nm)/SRO (30 nm)/STO (001) substrate, where SRO was used as a sacrificial layer. As indicated by the clear thickness fringes and a narrow rocking curve in the XRD pattern in Fig. S4, the SRO film has a high crystalline quality that is adequate for the subsequent growth of STO on top. Fig. 4(a) schematically shows the release process of STO membranes after the removal of SRO. A supporting layer, such as a polyamide (Kapton) tape on the slide glass, was attached to the STO/SRO/STO heterostructure, following which it was dipped into a 0.4 M $NaIO_4$ solution. After etching the SRO layer, a 500 nm–thick STO membrane was obtained on the Kapton tape. Fig. 4b shows an optical microscope image of the STO membrane. Notably, a millimeter-size crack-free membrane was obtained, as confirmed by optical microscopy (Fig. 4b) and SEM (Fig. 4c). Furthermore, the STO (002) reflection of the 500 nm–thick STO membrane appeared at a position identical to that for the STO single crystal, as shown in (Fig. 4d), revealing that the stoichiometry of the STO membrane was preserved.

It is noteworthy that the growth condition we found for stoichiometric STO films were reproducible; thus, they could be obtained in multiple samples (see the XRD patterns of STO layers in Fig. 1c, Fig. S1b, and Fig. S4a). However, our optimal laser ablation parameters and trend where lower laser energy density and smaller laser spot size are beneficial to stoichiometric STO films might vary in a different deposition system owing to differences in target-to-substrate distance, oxygen pressure, laser beam profile, etc. [44–46]. Nevertheless, we would emphasize that the growth window for obtaining stoichiometric STO films can be widened with the careful control of the laser energy density and laser spot size. As a consequence, the global attempts to widen the growth windows of thick oxide template layers will allow us to obtain functional complex oxide heterostructures incorporated on Si wafers through membrane transfer processes.

4. Conclusions

We fabricated a conducting interface between 4 nm–thick LAO and 500 nm–thick homoepitaxial STO films grown by PLD. With the optimized laser energy density and laser spot size on the STO target surface, the 500 nm–thick STO film did not show any lattice expansion within the resolution of XRD measurement. Temperature-dependent Raman spectroscopy further confirmed the structural identity between the thick stoichiometric STO film and single-crystal STO substrate. The interface at LAO/S-STO/STO exhibited a metallic behavior down to 4 K, similar to the typical LAO/STO heterostructure, while an insulating behavior was observed in LAO/Off-STO/STO owing to dominant defect scattering, which originated from cation off-stoichiometry in the STO film. By applying the optimal growth condition for homoepitaxial STO films found in this work to the growth of a 500 nm–thick STO film on top of SRO/STO, stoichiometric thick STO membranes with no lattice expansion could be obtained. This work offers a new opportunity to integrate complex oxide heterostructures into silicon technologies, which can provide a basis for the development of novel device applications.

CRediT authorship contribution statement

Jung-Woo Lee: Formal analysis, Data curation, Investigation, Writing – original draft. **Jongmin Lee:** Formal analysis, Data curation, Investigation, Writing – original draft. **Jamin Ahn:** Methodology, Data curation, Investigation. **Hongji Yoon:** Methodology, Data curation,

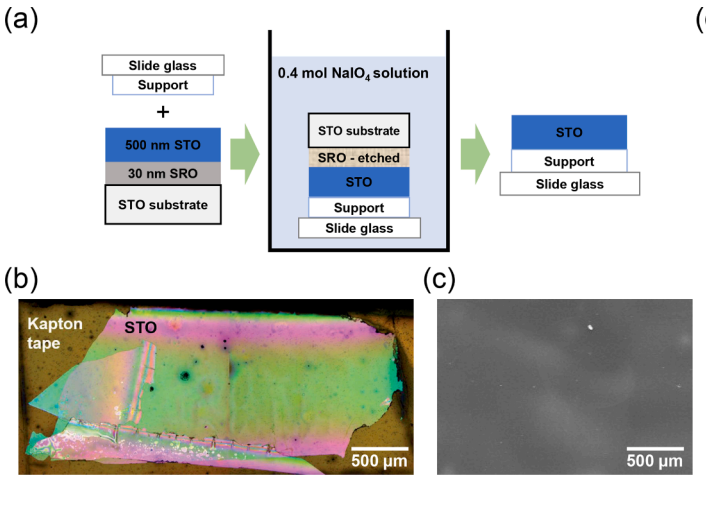

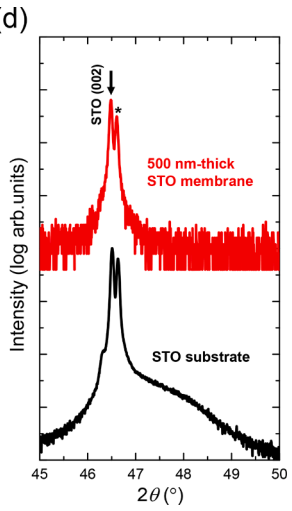

Fig. 4. (a) Schematic of the release process for fabricating STO membranes. (b) Optical microscope image of a 500 nm–thick STO membrane on Kapton tape. Because two different images emerged, they were combined, and the vertical line near the center of the membranes is an artifact of the combination and not a real feature. (c) SEM image of the 500 nm–thick STO membrane. (d) Out-of-plane θ-2θ XRD pattern of the STO membrane (red). Note that a high X-ray beam intensity, achieved by eliminating a four-bounce crystal monochromator, was needed for finding the reflection from the membrane. This results in the $K\alpha_2$ reflection, which is denoted as an asterisk. The XRD pattern of the bare STO substrate using the same beam and measurement conditions is also shown (black) for reference.

Investigation. **Hyunji An:** Methodology, Data curation, Investigation. **Sang-Il Park:** Methodology, Data curation, Investigation. **Hong-Seok Kim:** Methodology, Data curation, Investigation. **Sehun Seo:** Methodology, Data curation, Investigation. **Yong-Joo Doh:** Supervision. **Wooyoung Lee:** Supervision. **Sangwoo Ryu:** Conceptualization, Supervision, Funding acquisition, Writing – review & editing, Writing - original draft. **Sanghan Lee:** Conceptualization, Supervision, Funding acquisition, Writing – review & editing, Writing - original draft.

Declaration of Competing Interest

The authors declare that they have no known competing financial interests or personal relationships that could have appeared to influence the work reported in this paper.

Acknowledgements

This work was supported by the Creative Materials Discovery Program (No. 2017M3D1A1040834) through the National Research Foundation of Korea (NRF) funded by the Ministry of Science and ICT. This work was also supported by the Korea Institute of Energy Technology Evaluation and Planning (KETEP) and the Ministry of Trade, Industry & Energy (MOTIE) of the Republic of Korea (No. 20183010013880).

Appendix A. Supplementary material

Supplementary data to this article can be found online at https://doi.org/10.1016/j.apsusc.2022.152480.

References

[1] A.D. Caviglia, S. Gariglio, N. Reyren, D. Jaccard, T. Schneider, M. Gabay, S. Thiel, G. Hammerl, J. Mannhart, J.M. Triscone, Electric field control of the $LaAlO_3$/$SrTiO_3$ interface ground state, Nature 456 (2008) 624–627.
[2] L.F. Wang, Q.Y. Feng, Y. Kim, R. Kim, K.H. Lee, S.D. Pollard, Y.J. Shin, H.B. Zhou, W. Peng, D. Lee, W.J. Meng, H. Yang, J.H. Han, M. Kim, Q.Y. Lu, T.W. Noh, Ferroelectrically tunable magnetic skyrmions in ultrathin oxide heterostructures, Nat. Mater. 17 (2018) 1087–1094.
[3] J. Falson, D. Maryenko, B. Friess, D. Zhang, Y. Kozuka, A. Tsukazaki, J.H. Smet, M. Kawasaki, Even-denominator fractional quantum Hall physics in ZnO, Nat. Phys. 11 (2015) 347–351.
[4] A. Ohtomo, H.Y. Hwang, A high-mobility electron gas at the $LaAlO_3$/$SrTiO_3$ heterointerface, Nature 427 (2004) 423–426.
[5] H.Y. Hwang, Y. Iwasa, M. Kawasaki, B. Keimer, N. Nagaosa, Y. Tokura, Emergent phenomena at oxide interfaces, Nat. Mater. 11 (2012) 103–113.
[6] N. Reyren, S. Thiel, A.D. Caviglia, L.F. Kourkoutis, G. Hammerl, C. Richter, C. W. Schneider, T. Kopp, A.-S. Rüetschi, D. Jaccard, M. Gabay, D.A. Muller, J.-M. Triscone, J. Mannhart, Superconducting interfaces between insulating oxides, Science 317 (5842) (2007) 1196–1199.
[7] C. Cen, S. Thiel, G. Hammerl, C.W. Schneider, K.E. Andersen, C.S. Hellberg, J. Mannhart, J. Levy, Nanoscale control of an interfacial metal-insulator transition at room temperature, Nat. Mater. 7 (4) (2008) 298–302.
[8] J. Mannhart, D.G. Schlom, Oxide Interfaces-An Opportunity for Electronics, Science 327 (5973) (2010) 1607–1611.
[9] C. Cen, S. Thiel, J. Mannhart, J. Levy, Oxide Nanoelectronics on Demand, Science 323 (5917) (2009) 1026–1030.
[10] J.W. Park, D.F. Bogorin, C. Cen, D.A. Felker, Y. Zhang, C.T. Nelson, C.W. Bark, C. M. Folkman, X.Q. Pan, M.S. Rzchowski, J. Levy, C.B. Eom, Creation of a two-dimensional electron gas at an oxide interface on silicon, Nat. Commun. 1 (2010) 94.
[11] J.W. Reiner, A.M. Kolpak, Y. Segal, K.F. Garrity, S. Ismail-Beigi, C.H. Ahn, F. J. Walker, Crystalline Oxides on Silicon, Adv. Mater. 22 (2010) 2919–2938.
[12] R.A. McKee, F.J. Walker, M.F. Chisholm, Crystalline oxides on silicon: The first five monolayers, Phys. Rev. Lett. 81 (1998) 3014–3017.
[13] M.P. Warusawithana, C. Cen, C.R. Sleasman, J.C. Woicik, Y.L. Li, L.F. Kourkoutis, J.A. Klug, H. Li, P. Ryan, L.P. Wang, M. Bedzyk, D.A. Muller, L.Q. Chen, J. Levy, D. G. Schlom, A Ferroelectric Oxide Made Directly on Silicon, Science 324 (2009) 367–370.
[14] S.H. Baek, C.B. Eom, Epitaxial integration of perovskite-based multifunctional oxides on silicon, Acta Mater. 61 (2013) 2734–2750.
[15] L. Ji, M.D. McDaniel, S.J. Wang, A.B. Posadas, X.H. Li, H.Y. Huang, J.C. Lee, A. A. Demkov, A.J. Bard, J.G. Ekerdt, E.T. Yu, A silicon-based photocathode for water reduction with an epitaxial $SrTiO_3$ protection layer and a nanostructured catalyst, Nat. Nanotechnol. 10 (2015) 84–90.
[16] D. Lu, D.J. Baek, S.S. Hong, L.F. Kourkoutis, Y. Hikita, H.Y. Hwang, Synthesis of freestanding single-crystal perovskite films and heterostructures by etching of sacrificial water-soluble layers, Nat. Mater. 15 (2016) 1255–1260.
[17] A.K. Geim, K.S. Novoselov, The rise of graphene, Nat. Mater. 6 (3) (2007) 183–191.
[18] K.S. Novoselov, V.I. Fal'ko, L. Colombo, P.R. Gellert, M.G. Schwab, K. Kim, A roadmap for graphene, Nature 490 (7419) (2012) 192–200.
[19] B. Radisavljevic, A. Radenovic, J. Brivio, V. Giacometti, A. Kis, Single-layer MoS_2 transistors, Nat. Nanotechnol. 6 (3) (2011) 147–150.
[20] K.F. Mak, C. Lee, J. Hone, J. Shan, T.F. Heinz, Atomically Thin MoS_2: A New Direct-Gap Semiconductor, Phys. Rev. Lett. 105 (2010), 136805.
[21] D.M. Paskiewicz, R. Sichel-Tissot, E. Karapetrova, L. Stan, D.D. Fong, Single-Crystalline $SrRuO_3$ Nanomembranes: A Platform for Flexible Oxide Electronics, Nano Lett. 16 (1) (2016) 534–542.
[22] Z.Y. Chen, B.Y. Wang, B.H. Goodge, D. Lu, S.S. Hong, D.F. Li, L.F. Kourkoutis, Y. Hikita, H.Y. Hwang, Freestanding crystalline $YBa_2Cu_3O_{7-x}$ heterostructure membranes, Physical Review Materials 3 (2019) 060801(R).
[23] S.-I. Kim, H.-J. Choi, G. Lee, C.J. Roh, I. Jung, S.Y. Jung, R. Ning, S.O. Won, H. J. Chang, J.S. Lee, S.K. Kim, J.-S. Kim, C.-Y. Kang, J.-W. Choi, S.-H. Baek, 3D architectures of single-crystalline complex oxides, Mater. Horiz. 7 (6) (2020) 1552–1557.
[24] D. Li, S. Gariglio, C. Cancellieri, A. Fête, D. Stornaiuolo, J.-M. Triscone, Fabricating superconducting interfaces between artificially grown $LaAlO_3$ and $SrTiO_3$ thin films, APL Mater. 2 (1) (2014) 012102, https://doi.org/10.1063/1.4854335.
[25] K. Eom, M. Yu, J. Seo, D. Yang, H. Lee, J.-W. Lee, P. Irvin, S.H. Oh, J. Levy, C.-B. Eom, Electronically reconfigurable complex oxide heterostructure freestanding membranes, Science, Advances 7 (33) (2021), https://doi.org/10.1126/sciadv.abh1284.
[26] C.W. Bark, D.A. Felker, Y. Wang, Y. Zhang, H.W. Jang, C.M. Folkman, J.W. Park, S. H. Baek, H. Zhou, D.D. Fong, X.Q. Pan, E.Y. Tsymbal, M.S. Rzchowski, C.B. Eom, Tailoring a two-dimensional electron gas at the $LaAlO_3$/$SrTiO_3$ (001) interface by epitaxial strain, PNAS 108 (2011) 4720–4724.
[27] T. Ohnishi, K. Shibuya, T. Yamamoto, M. Lippmaa, Defects and transport in complex oxide thin films, J. Appl. Phys. 103 (2008), 103703.

[28] Y. Kozuka, Y. Hikita, C. Bell, H.Y. Hwang, Dramatic mobility enhancements in doped $SrTiO_3$ thin films by defect management, Appl. Phys. Lett. 97 (2010), 012107.
[29] F. Trier, D.V. Christensen, N. Pryds, Electron mobility in oxide heterostructures, J. Phys. D-Appl. Phys. 51 (29) (2018) 293002, https://doi.org/10.1088/1361-6463/aac9aa.
[30] D.G. Schlom, J.H. Haeni, J. Lettieri, C.D. Theis, W. Tian, J.C. Jiang, X.Q. Pan, Oxide nano-engineering using MBE, Materials Science and Engineering B-Solid State Materials for Advanced Technology 87 (2001) 282–291.
[31] B. Jalan, P. Moetakef, S. Stemmer, Molecular beam epitaxy of $SrTiO_3$ with a growth window, Appl. Phys. Lett. 95 (2009), 032906.
[32] B. Liu, V.R. Cooper, H.X. Xu, H.Y. Xiao, Y.W. Zhang, W.J. Weber, Composition dependent intrinsic defect structures in $SrTiO_3$, PCCP 16 (2014) 15590–15596.
[33] D. Lee, H.W. Wang, B.A. Noesges, T.J. Asel, J.B. Pan, J.W. Lee, Q.M. Yan, L. J. Brillson, X.F. Wu, C.B. Eom, Identification of a functional point defect in $SrTiO_3$, Physical Review Materials 2 (2018) 060403(R).
[34] C.M. Brooks, L.F. Kourkoutis, T. Heeg, J. Schubert, D.A. Muller, D.G. Schlom, Growth of homoepitaxial $SrTiO_3$ thin films by molecular-beam epitaxy, Appl. Phys. Lett. 94 (2009), 162905.
[35] D. Fuchs, M. Adam, P. Schweiss, S. Gerhold, S. Schuppler, R. Schneider, B. Obst, Structural properties of slightly off-stoichiometric homoepitaxial $SrTi_xO_{3-\delta}$ thin films, J. Appl. Phys. 88 (2000) 1844–1850.
[36] P.C. Dowden, Z. Bi, Q.X. Jia, Method for controlling energy density for reliable pulsed laser deposition of thin films, Rev. Sci. Instrum. 85 (2014), 025111.
[37] X. Wang, U. Helmersson, L.D. Madsen, I.P. Ivanov, P. Munger, S. Rudner, B. Hjorvarsson, J.E. Sundgren, Composition, structure, and dielectric tunability of epitaxial $SrTiO_3$ thin films grown by radio frequency magnetron sputtering, J. Vac. Sci. Technol., A 17 (1999) 564–570.
[38] T.R. Taylor, P.J. Hansen, N. Pervez, B. Acikel, R.A. York, J.S. Speck, Influence of stoichiometry on the dielectric properties of sputtered strontium titanate thin films, J. Appl. Phys. 94 (2003) 3390–3396.
[39] K. Orsel, R. Groenen, B. Bastiaens, G. Koster, G. Rijnders, K.J. Boller, Influence of the oxidation state of $SrTiO_3$ plasmas for stoichiometric growth of pulsed laser deposition films identified by laser induced fluorescence, APL Mater. 3 (2015), 106103.
[40] P.A. Fleury, J.M. Worlock, Electric-Field-Induced Raman Scattering in $SrTiO_3$ and $KTaO_3$, Phys. Rev. 174 (1968) 613–623.
[41] W.G. Nilsen, J.G. Skinner, Raman Spectrum of Strontium Titanate, J. Chem. Phys. 48 (1968) 2240.
[42] D.A. Tenne, A.K. Farrar, C.M. Brooks, T. Heeg, J. Schubert, H.W. Jang, C.W. Bark, C.M. Folkman, C.B. Eom, D.G. Schlom, Ferroelectricity in nonstoichiometric $SrTiO_3$ films studied by ultraviolet Raman spectroscopy, Appl. Phys. Lett. 97 (2010), 142901.
[43] Y. Matsubara, K.S. Takahashi, M.S. Bahramy, Y. Kozuka, D. Maryenko, J. Falson, A. Tsukazaki, Y. Tokura, M. Kawasaki, Observation of the quantum Hall effect in delta-doped $SrTiO_3$, Nat. Commun. 7 (2016) 11631.
[44] T. Ohnishi, M. Lippmaa, T. Yamamoto, S. Meguro, H. Koinumab, Improved stoichiometry and misfit control in perovskite thin film formation at a critical fluence by pulsed laser deposition, Appl. Phys. Lett. 87 (2005), 241919.
[45] H.N. Lee, S.S.A. Seo, W.S. Choi, C.M. Rouleau, Growth control of oxygen stoichiometry in homoepitaxial $SrTiO_3$ films by pulsed laser epitaxy in high vacuum, Sci. Rep. 6 (2016) 19941.
[46] J. Schou, Physical aspects of the pulsed laser deposition technique: The stoichiometric transfer of material from target to film, Appl. Surf. Sci. 255 (2009) 5191–5198.